

Supporting Information

Puchner et al. 10.1073/pnas.1309676110

SI Materials and Methods

Sample Preparation. Yeast strains (Tables S1–S3) were grown at 30 °C overnight in synthetic SD medium, diluted 1:50 in SD, and grown for 3–4 h to log phase in the dark. To avoid bleaching and preactivation of mEos2, exposure of the cells to light was minimized for all following steps. The chambered borosilicate coverglasses (eight-well, Lab-Tek II, 155409; Sigma-Aldrich) were incubated with 1 M HCl for 10 min, washed three times with double-distilled H₂O (ddH₂O) (Millipore) and then incubated with an aqueous and sterile filtered solution of 0.8 mg/mL Con A (Sigma-Aldrich) for at least 30 min. After washing three times with ddH₂O, yeast cells were incubated on the coverglass and allowed to settle for 30–45 min in SD at pH 7.5 (adjusted with monobasic potassium phosphate KH₂PO₄ and K₂HPO₄). For fixation, formaldehyde [37% (vol/vol); Sigma-Aldrich] was directly added to the chambers to a final concentration of 4% (vol/vol) for 30 min. Fixation with glutaraldehyde 0.2% results in high blinking background and cannot be used for single-molecule localization microscopy. We note that immobilization before fixation is crucial for achieving best immobilization of the cells. After gentle washing with SD three times, cells were imaged.

Experimental Setup and Data Acquisition. Superresolution microscopy experiments were performed on a custom-built microscope as previously described (1). The microscope is based on a Nikon Ti-E inverted microscope with the Perfect Focus System. Four activation/imaging lasers (Stradus 405-100, Stradus 488-50, and Stradus 642-110; Vortran Laser Technology and Sapphire 561-200-CW; Coherent) are combined using dichroic mirrors, aligned, expanded, and focused to the back focal plane of the objective (Olympus ×100 UPlanSApo N.A. 1.4). The Stradus lasers are controlled directly by the computer, whereas the Sapphire 561-nm laser is shuttered using an acoustic optical modulator (Crystal Technology). A quadband dichroic mirror (zt405/488/561/640rpc; Chroma) and a band-pass filter (ET595/50m; Chroma) separate the fluorescence emission from the excitation light. The images were recorded at a frame rate of 57 Hz on an electron multiplying CCD camera (Ixon+ DU897E-CS0-BV; Andor). The camera was cooled down to –68 °C and the amplifying gain was set to 30. To estimate the used power density for the activation and excitation laser, we measured the power in the back focal plane of the microscope and divided it by the illuminated area. The typical power density for the 561-nm excitation was ~1 kW/cm² (power 17 mW) and for the 405-nm activation in a range between 0.06 W/cm² and 6 W/cm² (at a power between 1–100 μW). During image acquisition, the axial drift of the microscope stage was stabilized by the Perfect Focus System. To correct for the lateral stage drift, we installed a light-emitting diode (LED) light as the transmitted light source for the microscope. During every 10th frame of image acquisition, we turned the 561-nm excitation laser off and the LED on so that a bright-field image of the sample was recorded. In the same frames also the 405-nm activation laser was turned on to activate a very small subpopulation of mEos2 molecules. The activation power was adjusted over time to achieve a sparse and constant switching rate per frame. Both data acquisition and analysis were performed using custom-written software.

For conventional fluorescence images of GFP-tagged proteins we used a 488-nm laser and a power density of 6 W/cm² (power 100 μW) on the same microscope setup using a band-pass filter to separate the fluorescence from excitation light (ET525/50m; Chroma). We recorded 50 images at a frame rate of 5 Hz and averaged the images for a better signal-to-noise ratio.

Basic Image Analysis. A typical superresolution image was generated from a sequence of 20,000–50,000 image frames, recorded at 57 Hz. The movie consists of a repetitive sequence of activation frames (every 10th frame activation laser and LED are turned on) and imaging frames (the following nine frames with the excitation laser turned on). For each imaging frame, fluorescent spots were identified and fit to an elliptical Gaussian function to determine their centroid positions, intensities, widths, and ellipticities. Based on these parameters, peaks too dim, too wide, or too elliptical to yield satisfactory localization accuracy were rejected from further analysis. For all localizations the fit parameters such as the *x* and *y* coordinates, photon number, background photons, and frame of appearance were saved in a molecule list for further analysis. Besides the number of photons detected from each molecule, another factor that limits the localization accuracy was sample drift during the course of the experiment. By correlating the LED bright-field images recorded in each 10th frame and by tracking the centroid of the correlation function, the sample drift was determined and subtracted from the *x* and *y* coordinates of all localizations.

For image presentation, each localization point was either represented by a small marker (e.g., a cross) or rendered as a normalized 2D Gaussian peak. The total number of photons detected from each switching cycle was used as an additional filter for image presentation to reject localizations with low accuracy (<250 photons). However, for quantitative analysis all localizations without applying a photon threshold were considered.

Photophysical Characterization of mEos2, Blink Correction, and Cluster Algorithm. For all following data analysis and correction steps, the molecule list from the analysis software including all relevant fit parameters (coordinates of localizations, number of photons, width, height, frame, etc.) was imported and processed by custom-written procedures in Igor Pro-6.0 (Wavemetrics).

Pair-correlation function. The pair-correlation function (PCF) was calculated by creating a histogram (*H*) from the distances between all points *N* (either the coordinates of fluorescent bursts or the corrected single molecule positions), and by dividing each bin by *N* and the area at the distance *r_i*:

$$PCF(r_i) = \frac{H(r_i)}{N \times (\pi(r_i + \Delta r)^2 - r_i^2)},$$

where *H_i* is the bin *i* of the distance histogram, *r_i* the distance of bin *i*, and Δr the bin width.

We note that the PCF of the single repeat in Fig. 1B only looks flat if the top or bottom of the cell membrane is imaged and molecules are randomly distributed in two dimensions. If a section of the cell is imaged, the circular distribution causes a slight peak of the PCF, which was confirmed by simulations. However, the amplitude of the peak is smaller compared the one of protein complexes with higher stoichiometry. We note that we did not normalize the PCF by the average density as is often done to keep the information about the absolute molecule densities.

Dark-time histogram. To characterize the photophysical parameters of mEos2, single-molecule superresolution data were recorded with the calibration strain expressing mEos2 fused to the Pleckstrin homology (PH) domain of Plcδ at very low levels under control of a truncated version of the weak INO4 promoter (2). Owing to the truncation, this promoter results in expression levels on the order of hundreds of [PH]₂-mEos2 molecules per

cell (2, 3) that are spatially well separated (Fig. 1). The spread of fluorescent bursts originating from single molecules can be calculated by the radial distribution function, resulting in a maximum spread of 150 nm (PCF in Fig. 1*B*, *Top*). Therefore, bursts appearing within a distance of 150 nm were grouped (details regarding grouping are given below) and a histogram of dark times was obtained (Fig. S1). Integrating and normalizing the dark-time histogram allows us to determine the 99% quintile (meaning that 99% of bursts have a dark time shorter than the cutoff), which is under our experimental conditions 2.66 s.

Blink correction. Using the experimentally determined spread of localizations from single molecules (150 nm) as well as the 99% quantile for the dark-time cutoff (2.66 s), fluorescent bursts originating from the same molecule can now be correctly combined and averaged (Fig. S1). First, it is determined whether two consecutive localizations appear within 150 nm and 2.66 s. If so, they get combined to a photon-weighted average position having the sum of photons associated with it. If a third localization again appears within the cutoff time with respect to the preceding one and within 150 nm compared with the averaged position, a new photon-weighted average position is calculated from the old average position and the third localization. This iterative process ensures that at each step the maximum information (photons) is used and it is repeated until all localizations are averaged to the new molecule's position.

Whereas blink correction and counting small numbers of molecules is straightforward, it is expected that the fluorescence of different mEos2 molecules may start to overlap in space and time, which leads to undercounting (4). To verify that our method still holds for the highest labeling densities of several hundred mEos2 molecules/vesicle in this study, we plotted the total number of fluorescent bursts from individual FYVE–mEos2-associated vesicles against the corrected number of molecules (Fig. S1*C*). For small molecule numbers, the number of fluorescent bursts shows a large spread owing to the stochastic blink behavior, highlighting the need for blink correction. For larger molecule numbers (>100), the ensemble is large enough so that stochastic blink behavior averages out. Most importantly, the relation of the number of bursts and molecule number is still linear, which shows that even for hundreds of mEos2 molecules undercounting owing to overlap of their fluorescence in time is not significant.

Counting histograms and noise. To count molecules in protein complexes in an unbiased way, we used a counting algorithm that considers all molecules in a superresolution image and determines the stoichiometry based on intermolecular distances. In protein complexes with a small dimension below the resolution (e.g., triple repeat of mEos2), the spread of molecules is given by the experimental resolution itself. As seen by the PCF of the double and triple mEos2 repeat in Fig. 1*B*, the maximum spread is clearly below 100 nm (also for 2× repeat). For such protein complexes, molecules within a radius of 50 nm were therefore assigned to one cluster. For the grouping itself, the same procedure as for blink correction was used except that regular averaging instead of photon-weighted averaging was used to find the center of a cluster.

Fluorescent background of yeast cells was minimized by the use of synthetic SD medium, optimization of fixation, and excitation power. We obtain a very low noise level of 0.8 counts per square micrometer per 10,000 frames by measuring background in yeast cells lacking mEos2 under imaging conditions (Fig. S2) and by blink correction of the noise with the same parameters as the actual data. In the case of individual endocytic vesicles where an area of less than 0.5 μm^2 is selected for analysis, this results on average in two misidentified molecules owing to background noise. However, for the automated, unbiased analysis of the calibration strains in Fig. 1, the area covered by the whole cell contributes to the noise. This sparse and randomly distributed

noise only appears as individual counts in counting histograms. To properly correct for those noise counts in the actual data, the counting histograms were normalized by the number of total frames and the area from which counts were detected (dashed lines in images in Fig. S2). After subtracting the equally normalized noise histogram, the counting histograms were rescaled again by the area and number of frames to obtain absolute counts (Fig. S2, *Right*).

Analysis of vesicle size and number of FYVE domains. For the analysis of vesicle size and number of associated FYVE domains, super-resolution data were blink-corrected as described earlier, and only structures with more than three molecules were used for further analysis. To calculate the surface area of vesicles, we used the average SD of FYVE–mEos2 molecules in x and y as a radius and assumed a spherical shape in three dimensions. The resulted error of the calculated surface compared with the exact one of an ellipsoid is smaller than the error owing to our localization precision of 20 nm, even for a theoretical elliptical shape with a main axis ratio of 2:1. For vesicles with a very low number of phosphatidylinositol 3-phosphate (PI3P) binding sites (<10) the actual size of vesicles may be underestimated owing to an uneven distribution of mEos2 molecules. Also for very large and uneven multivesicular structures (e.g., YPT7 associated in Fig. 5*A*), the surface area is underestimated to some extent. However, this only compresses the endocytic trajectory for large structures and does not change its branching point.

We note that the probability of overlap between two molecules in time is low owing to the long experimental time (about 40,000 frames per 700 s) and low labeling densities in this study. This notion is confirmed by plotting the number of molecules on individual endocytic vesicles against the total number of fluorescent bursts in Fig. S1. For small numbers of molecules the stochastic blink behavior of mEos2 causes a spread, highlighting the necessity for blink correction. For larger numbers of molecules, this spread becomes smaller because it averages out owing to the larger ensemble. Importantly, even for >100 molecules, the number of bursts vs. molecules stays quite linear, showing that undercounting due to temporal overlap between molecules is low. We note that in experiments with very dense structures like the spindle pole body (>1,500 observed molecules, 40,000 frames), the blink correction with parameters used in this study results in undercounting owing to temporal overlap. In such dense samples either the data recording time needs to be enlarged and 405-nm activation lowered to avoid temporal overlap or the total number of fluorescent bursts needs to be used as an ensemble value to calculate the number of molecules.

Combined Superresolution and Conventional Fluorescence Imaging.

For colocalization studies (Figs. 3 and 5), we combined conventional quantitative fluorescence imaging with GFP and super-resolution with mEos2. Because fixed yeast cells exhibit too high fluorescent and blinking background in the GFP channel for single-molecule imaging with available photoswitchable fluorescent proteins (PAFPs), the combined conventional approach is a robust solution with the same information two-color super-resolution microscopy would provide: the amount of the GFP- and mEos2-labeled proteins on a vesicle and its size.

Because mEos2 fluoresce in the GFP channel in its pre-activated state, we recorded the GFP signal before and after imaging with mEos2. Although the approach of extensive mEos2 activation to the red state and imaging before imaging in the GFP channel has already been successfully applied for two-color super-resolution imaging with mEos2, we found that even in the preactivated state the cross-talk is less than 10% (Fig. S3). After mEos2 imaging, the faint signal in the GFP channel vanished, which indicates that all mEos2 molecules were activated and imaged (Fig. S3, *Right*).

To obtain quantitative GFP images, the average camera noise was subtracted from the recorded data before division by a flat field (recorded with 100-nM fluorescein; Sigma-Aldrich) to account for uneven illumination. To determine the amount of GFP per vesicle, we used two methods: Each vesicle was fitted by a Gaussian function whose volume is a measure of the amount of GFP and the intensity of pixels under the fit was summed up. Because these two methods give slightly varying results for very bright and faint vesicles we used the average of both values as a more confident value. All GFP values presented for colocalization were taken from data recorded after mEos2 imaging.

In the conventional GFP images sometimes vesicles above and below the focal plane are visible, whereas in the single-molecule mEos2 channel only a thin slice of about 500 nm thickness is

imaged. Therefore, we used the mEos2 channel as a guide and analyzed only those vesicles showing at least three mEos2 molecules. The colocalization of the FYVE domain with the three protein markers (Fig. S4 and Fig. 5) corresponds well to the current model of the endocytic pathway. Clathrin exhibits a clear anticorrelation with the FYVE domain: It only colocalizes with vesicles having small amounts of FYVE molecules (<50) and vesicles with a high number of FYVE molecules (>50) show no colocalization, except one outlier slightly above the GFP threshold (Fig. S4). Vps21 is associated with vesicles and early endosomes having an intermediate number of FYVE molecules, and YPT7 is only associated with structures having the highest amount of FYVE domains. In Fig. 5B only vesicles with a clear colocalization signal above the 90% threshold (Fig. S4A) are displayed and cover the whole endocytic trajectory.

1. Beaudoin GM, 3rd, et al. (2012) Afadin, a Ras/Rap effector that controls cadherin function, promotes spine and excitatory synapse density in the hippocampus. *J Neurosci* 32(1):99–110.
2. Robinson KA, Lopes JM (2000) The promoter of the yeast *INO4* regulatory gene: A model of the simplest yeast promoter. *J Bacteriol* 182(10):2746–2752.
3. Ghaemmaghami S, et al. (2003) Global analysis of protein expression in yeast. *Nature* 425(6959):737–741.
4. Annibale P, Vanni S, Scarselli M, Rothlisberger U, Radenovic A (2011) Quantitative photo activated localization microscopy: Unraveling the effects of photoblinking. *PLoS ONE* 6(7):e22678.

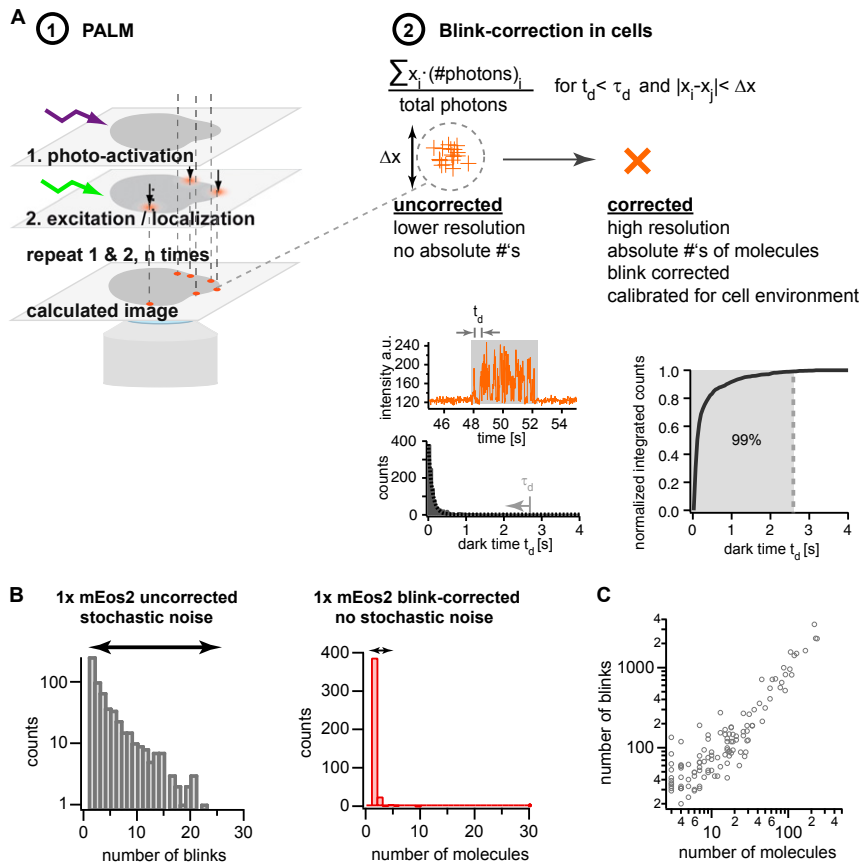


Fig. S1. Schematic of experimental setup and blink correction. (A) (Left) Single-molecule superresolution microscopy localizes fluorescent bursts from single PAFPs with high accuracy by fitting their intensity profile. A small subset of PAFPs is stochastically activated by 405-nm light and consecutively excited and imaged. Activation and excitation cycles are repeated until all molecules are imaged and bleached. All localizations are superimposed in the final super-resolution image. (Right) Blink correction with parameters determined under imaging conditions in cells. In uncorrected images, each fluorescent burst produces a localization, causing a single molecule to appear as a cluster. In corrected images, fluorescent bursts from the same molecule (dark time $t_d < \tau_d$ and $|x_i - x_j| < \Delta x$) are combined to the photon-weighted average position. The dark-time histogram was obtained from the $[\text{PH}]_2$ -1xEos2 construct and the cutoff was determined by the 99% quantile to be 2.66 s, corresponding to 150 frames. For Δx 150 nm was used because bursts from the same molecule fall within this distance (see PCF, Fig. 1B). (B) In uncorrected data, the broad distribution of the number of fluorescent bursts per mEos2 molecules makes it impossible to count molecule numbers. In contrast, blink-corrected data show mostly a single spike at 1 with a small number of double counts if two molecules are in close proximity. (C) To verify that our counting method holds even for a large number of molecules, we plotted the number of observed fluorescent bursts of individual vesicles with associated FYVE-mEos2 molecules against the number of blink-corrected molecules. For small molecule numbers (< 100), the stochastic blink behavior causes a broad spread of bursts, highlighting the need for blink correction. For larger molecule numbers the ensemble gets large enough so that fluctuations in the number of bursts average out. Most importantly, the relationship stays linear, showing that no significant undercounting owing to overlap of the fluorescence of two molecules in time takes place.

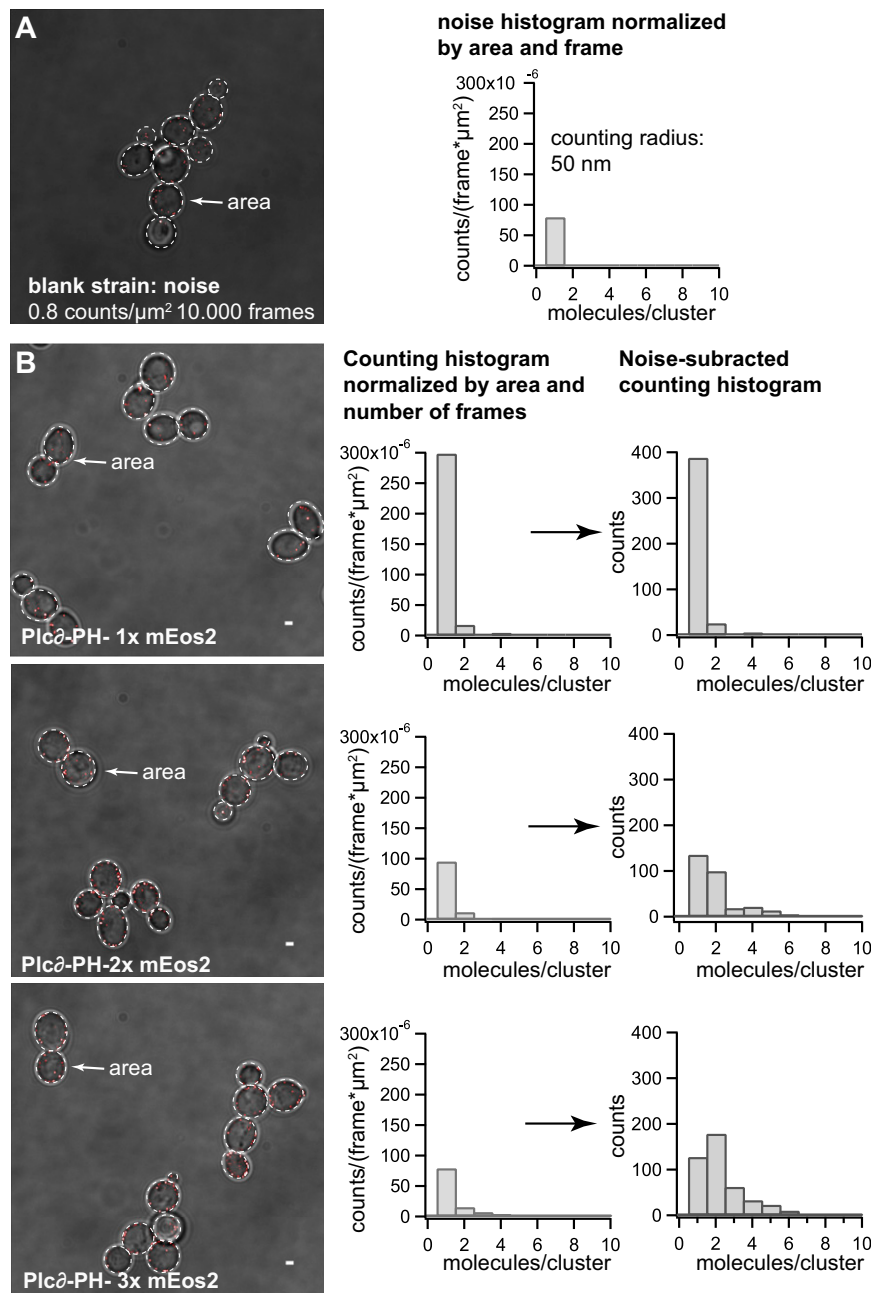


Fig. S2. Noise analysis and subtraction from counting histograms. (A) Cells without mEos2 were imaged and analyzed under the same conditions as the actual experiments revealing low blinking background noise, which is randomly distributed within the cells. Accordingly, the counting histogram (*Right*) displays only single noise counts. To subtract this additive noise from counting histograms of the calibration constructs (B), histograms were normalized by the total number of frames and the area of cells from which signal was detected. For the single, double, and triple repeats, the maximum distance of molecules belonging to the same cluster was 50 nm (see PCF, Fig. 1), and accordingly the normalized noise histogram with a 50-nm counting radius was subtracted. After noise subtraction, counting histograms from the same construct were multiplied by the number of frames and area to obtain absolute molecule numbers and summed to the final histogram showing the absolute number of noise-corrected molecule counts (*Right*).

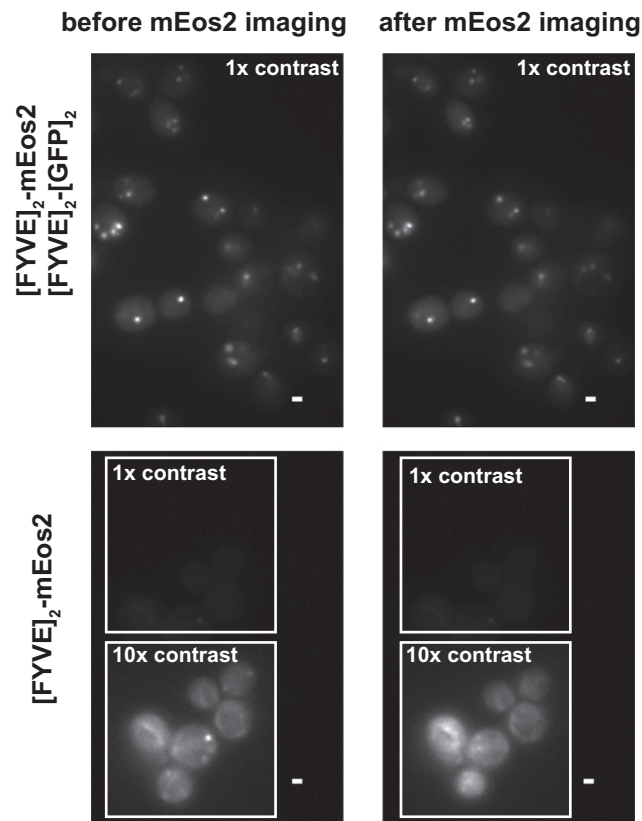


Fig. S3. Low cross-talk of mEos2 in GFP channel after complete mEos2 imaging. Images from the strain expressing the FYVE domain fused to mEos2 and to GFP show high *s/n* in the GFP channel before and after mEos2 imaging (*Upper*). In contrast, the strain expressing FYVE–mEos2 alone shows low cross-talk into the GFP channel (<10%), which is barely above the background fluorescence even for hundreds of mEos2 molecules (*Lower*). After mEos2 imaging the faint signal from the brightness vesicles disappears, showing that all mEos2 molecules were photoactivated and imaged. (Scale bars, 1 μm .)

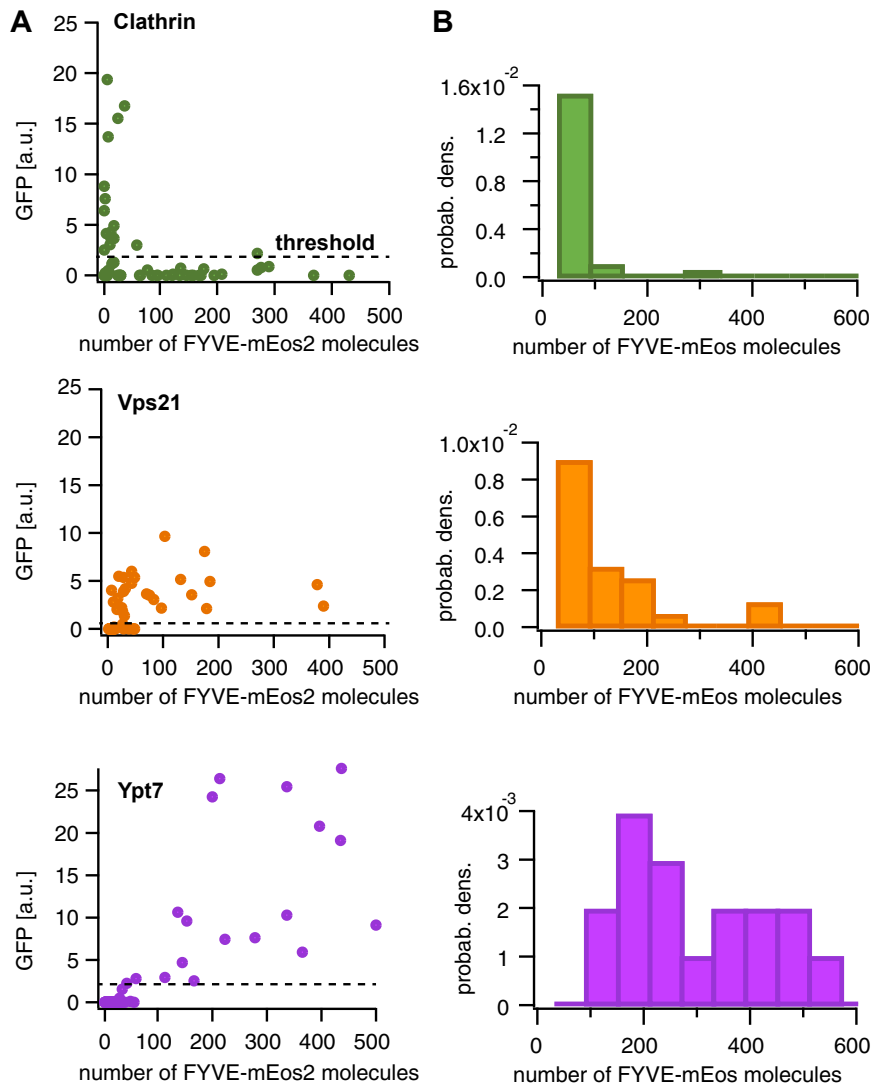


Fig. S4. Colocalization of endocytic/endosomal landmark proteins with PI3P reporter. (A) By plotting the total GFP intensity of each vesicle against the number of FYVE-mEos2 molecules, we obtain characteristic colocalization patterns for each class of endocytic/endosomal proteins, which correspond well with the current model: Clathrin colocalizes only with vesicles having very low PI3P binding sites. In the case of Vps21, vesicles with low to intermediate PI3P binding sites display partial colocalization; high colocalization is found for vesicles with intermediate PI3P binding sites. Ypt7 only colocalizes with vesicles/endosomes displaying intermediate to highest PI3P binding sites. In the histograms (B) and colocalization in Fig. 5B only vesicles above the indicated threshold (10% of maximum signal) are displayed.

